JPhys Energy

PAPER • **OPEN ACCESS**

Thermal and electronic transport properties of $ACrX_2$ superionic conductors (A=Cu, Ag and X=S, Se)

To cite this article: Md Towhidur Rahman *et al* 2025 *J. Phys. Energy* **7** 035016

Journal of Physics: Energy

PAPER

Thermal and electronic transport properties of $ACrX_2$ superionic conductors (A=Cu, Ag and X=S, Se)

Md Towhidur Rahman[1], Kamil Ciesielski[3], Joseph Pelkey[2], A K M Ashiquzzaman Shawon[2], Eric Toberer[3] and Alexandra Zevalkink[2,*]

[1] Department of Mechanical Engineering, Michigan State University, East Lansing, MI, United States of America
[2] Department of Chemical Engineering and Materials Science, Michigan State University, East Lansing, MI, United States of America
[3] Department of Physics, Colorado School of Mines, Golden, CO 80401, United States of America
[*] Author to whom any correspondence should be addressed.

E-mail: alexzev@msu.edu

Keywords: superionic conductivity, transport properties, lattice thermal conductivity, thermoelectrics

Supplementary material for this article is available online

OPEN ACCESS

RECEIVED
19 October 2024

REVISED
15 May 2025

ACCEPTED FOR PUBLICATION
2 June 2025

PUBLISHED
17 June 2025

Abstract

Superionic conductors, including $ACrX_2$ (A=Ag, Cu; X = S, Se) compounds, have attracted attention due to their low lattice thermal conductivity and high ionic conductivity. These properties are driven by structural characteristics such as anharmonicity, soft bonding, and disorder, which enhance both fast ion transport and thermal resistance. In the present study, we investigate the impact of various factors (e.g. A-site disorder, microstructure, speed of sound and chemical composition) on the thermal conductivity of the compounds $CuCrS_2$, $CuCrSe_2$, $AgCrS_2$ and $AgCrSe_2$. The samples were synthesized using solid state reaction, ball milling and subsequent spark plasma sintering, and thermal diffusivity, electrical resistivity, Hall coefficients and Seebeck coefficients were measured as a function of temperature. The selenides were found to behave as degenerate semiconductors, with reasonable thermoelectric figure of merit (up to 0.79 in $CuCrSe_2$), while the sulfides behaved as non-degenerate semiconductors with high electrical resistivity. At room temperature, all samples are in the ordered phase and show low lattice thermal conductivity ranging from 0.60 W m^{-1}-K in $AgCrSe_2$ to 1.1 W m^{-1}-K in $CuCrSe_2$. Little reduction in lattice thermal conductivity was observed in the high-temperature phase, despite the increased disorder on the cation site and the onset of superionic conductivity. This suggests that the low lattice thermal conductivity in $ACrX_2$ compounds is an inherent property of the crystal structure, caused by anharmonic bonding and diffuson dominated transport.

1. Introduction

In energy storage and conversion devices, controlling thermal and ionic conductivity is critical for optimizing performance. Superionic conductors (SICs) are a class of materials that exhibit both high, liquid-like diffusivity of the mobile ions [1–5] and simultaneously, exceptionally low lattice thermal conductivity [6]. As battery materials, the high ionic conductivity of SICs is ideal for efficient charge transport, while the low thermal conductivity is a major drawback that can lead to poor heat management in devices [7]. *Conversely*, as thermoelectric materials, the low thermal conductivity of SICs is attractive [8], while the high ionic conductivity can be a serious cause of performance degradation [6], and their efficiency is crucial for process sustainability when large-scale implementation is considered [9]. Clearly, understanding the link between thermal and ionic conductivity—and potentially decoupling them—is needed for advancing the field and paving the way for more versatile materials in energy applications.

The study of $ACrX_2$ compounds (A=Ag, Cu; X=S, Se) as thermoelectrics has gained momentum recently, because the same structural characteristics responsible for their fast ion transport (e.g. soft bonding, high anharmonicity, and disorder) are thought to be responsible for their low lattice thermal conductivity

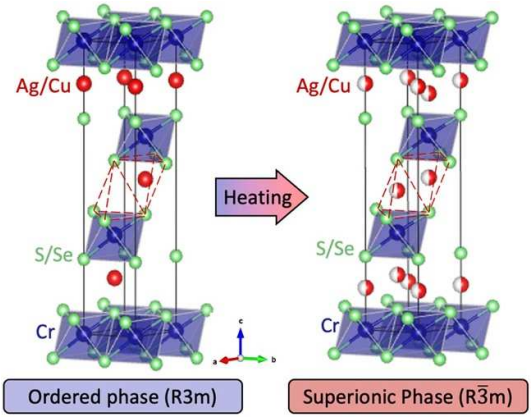

Figure 1. Crystal structure of $ACrX_2$ compounds (A = Ag, Cu; X = S, Se) in the ordered (left) and disordered (right) phase. Ag/Cu cations are shown in red; S/Se anions are in light green and Cr ions are in blue. CrX_6 octahedral sites are shaded in blue, while the dashed orange line shows AX_4 tetrahedral sites. The mixed half red-white spheres indicate 50% occupancy at the cation sites. The structure is in ordered phase below superionic transition temperature (for example, 475 K for $AgCrSe_2$), one of the tetrahedral sites remain empty. But above that temperature, both the sites are half filled (50% probability of occupancy) with the cations, and the structure enters superionic phase.

[10–12]. $ACrX_2$ compounds have a simple layered structure (shown in figure 1), defined by alternating edge-sharing octahedral CrX_6 layers and half-filled AX_4 tetrahedral layers. In the room temperature phase (space group $R3m$), the A atoms fully occupy every second AX_4 tetrahedral site. Above the superionic phase transition (SIT) temperature, the symmetry increases ($R3m \rightarrow R\bar{3}m$) as the A atoms diffuse into the empty neighboring tetrahedral sites, resulting in 50% occupancy of all tetrahedral sites [10, 13]. The transition temperatures (T_c) of $CuCrSe_2$ and $AgCrSe_2$ have been reported to be at around 365 K [14] and 475 K [15, 16], respectively. Replacing Se with S increases the transition temperature to around 668 K and 688 K for $AgCrS_2$ and $CuCrS_2$, respectively [17]. The transition temperature variation influences the efficient operating range for potential applications. Generally, lower transition temperatures mean they can achieve high ionic mobility at lower operating temperatures. Other Ag-conducting SICs such as Ag_2S, Ag_2Se and AgI have Tc > 400 K [18–20], which are comparable with the transition temperature range of the $ACrX_2$ compounds.

SICs are often described as crystalline materials possessing mobile, liquid-like sublattices that are responsible for their high ionic diffusivity. Indeed, above the superionic transition temperature, the ionic diffusivities in $ACrX_2$ compounds have been reported to increase significantly [21]. However, while the 'liquid-like' description of the Cu or Ag sublattice may be a convenient concept for explaining high ionic conductivity, it is not clear whether 'liquid-like' accurately describes the lattice dynamics or thermal properties of this class of compound. A liquid-like sublattice would imply fluid motion of ions (as opposed to hopping between distinct sites) and therefore complete suppression of transverse phonons. Early reports supported this picture. Li *et al* [13] claimed that the transverse acoustic phonons in $AgCrSe_2$ are completely suppressed in the high temperature phase by ultrafast dynamic disorder. Measurements by Li *et al* [13] and by Gascoin *et al* [8] further suggested that the heat capacity drops below the Dulong–Petit value at high temperature, which was cited by Bailey *et al* as further evidence of liquid-like dynamics [22]. However, later results from Bhattacharya *et al* reported measurements of heat capacity in $AgCrSe_2$ and $CuCrSe_2$ [11] that were approximately equal to the Dulong Petit (DP) limit. More importantly, later INS studies [10, 14, 17] showed that while the most non-dispersive transverse phonons are suppressed in the disordered phase, the more dispersive low-frequency transverse phonons persist in the disordered phase of $ACrX_2$ compounds. Similar results have been reported in other classes of SICs [23, 24].

The present study aims to answer the question: what is the impact of the order–disorder transition on the lattice thermal conductivity of $ACrX_2$ compounds? The works described above attributed the intrinsically low thermal conductivity of $ACrX_2$ compounds to the breakdown of the transverse phonon modes observed in the disordered phase. For $AgCrSe_2$ and $CuCrSe_2$, however, prior reports have *not* shown evidence of a decreased κ_l at temperatures *above* the phase transition. Indeed, κ_l was reported to be nearly temperature independent in both selenides across the entire measured range [6, 25]. Studies of the transport properties of $AgCrS_2$ and $CuCrS_2$ compounds have been limited to a few studies [12, 26, 27], while Rana *et al* [28] linked phonon scattering to ultra-low lattice thermal conductivity in the $ACrSe_2$ samples. There have been few reports on first-principles studies on phonon scattering, anharmonicity and thermal transport property [29, 30]. Here, we investigate the impact of the order–disorder phase transition on the electronic and thermal transport properties of the four different compounds, $AgCrS_2$, $AgCrSe_2$, $CuCrS_2$ and $CuCrSe_2$. We also

consider differences in the microstructure and speed of sound of the samples. The high-temperature electronic and thermal properties of the sulfides are reported here for the first time. This series of compounds allows us to systematically examine the relationship, if any, between the disorder on the cation sublattice, the breakdown of transverse acoustic phonons and the resulting thermal conductivity of these materials.

2. Materials and method

2.1. Synthesis

Polycrystalline $AgCrSe_2$, $CuCrSe_2$, $AgCrS_2$ and $CuCrS_2$ samples were synthesized by solid state reaction, following slightly different routes for each sample individually. The corresponding stoichiometric amounts of Ag (shots, Sigma-Aldrich, 99.99% purity), Cu (powder, Alfa-Aesar, 99.9% purity), Cr (chips, Sigma-Aldrich, 99.995% purity), Se (shot, Alfa-Aesar, 99.999% purity) and S (shot, Alfa Aesar, 99.999% purity) were weighed in an argon-filled glovebox. For $AgCrSe_2$, the weighed elements were sealed in a quartz ampoule under static vacuum, heated up to 1173 K at 1 K min^{-1} rate for 24 h, followed by slow cooling in 12 h, and finally hand-ground by mortar and pestle into fine powder inside the glovebox [15]. A similar procedure was used for $AgCrS_2$, except that the elements were heated up to 1273 K and held at that temperature time for 48 h [31, 32]. For both samples, phase-pure fine powders were obtained and confirmed with x-ray diffraction. The powders were then compacted by Spark Plasma Sintering (SPS) at 873 K for 20 min ($AgCrSe_2$) and 1023 K for 30 min ($AgCrS_2$) to get consolidated dense pucks.

For $CuCrS_2$, elemental Cu, Cr and S were heated up to 1173 K, with a holding time of 48 h, in a vacuum sealed ampoule, hand-ground, and spark plasma sintered at 1023 K for 30 min [33] to obtain phase purity and relative density higher than 95%. We note that due to the high vapor pressure of sulfur, only 2 grams of sample were synthesized in a single batch to avoid explosion of quartz tubes during furnace heating. The synthesis route for $CuCrSe_2$ involved an initial ball-milling step, which is reported to help avoid formation of $CuCr_2Se_4$ as a secondary phase [34]. Inside an argon-filled glovebox, the elements were sealed in stainless steel SPEX vials. 10 grams of powder were then ball milled with three 7/16”-stainless steel ball bearing for 3 h using SPEX SamplePrep 8000D. After milling, approximately 93% of the initial load was recovered. The powder was vacuum sealed in a quartz ampoule, heated to 973 K, held for 4 h and air quenched. Lastly, the sample was ground by mortar and pestle and spark plasma sintered at 873 K for 20 min to obtain a phase pure consolidated sample [34].

2.2. X-ray diffraction

X-ray diffraction (XRD) was performed on polycrystalline spark plasma sintered samples using a Rigaku SMARTLAB diffractometer with a Cu–Kα radiation source. XRD was also used in between each synthesis step to track the phase purity of the obtained powders. $AgCrSe_2$ and $AgCrS_2$ were phase pure before SPS, but for $CuCrSe_2$ and $CuCrS_2$, the samples were observed to be single phase afterwards. The lattice parameters of the SPS processed consolidated pucks were obtained by Rietveld refinement using the Rigaku PDXL-2 software. Scanning electron microscopy (SEM) was conducted on fractured sample surfaces parallel to SPS direction using an AURIGA-Crossbeam Workstation Dual Column SEM.

2.3. Thermal and electronic transport measurements

Thermal diffusivity (D) was measured during the heating and cooling cycle using a NETZSCH Light Flash Apparatus (LFA) 467 HyperFlash. Thermal conductivity (κ_{total}) was calculated using the equation $\kappa_{total} = \varrho \times D \times C_p$, where D is the thermal diffusion, ρ is the geometric density and C_p is the constant pressure heat capacity computed with the Dulong–Petit approximation. The resistivity and Hall effect were collected on a custom-built apparatus [35] using Van der Pauw technique. The current supplied was 150 mA, while the magnetic field amounted to 1 T. Seebeck coefficient was also studied on home-built apparatus [36]. For both electronic measurements, heating and cooling curves were checked to ensure lack of thermal hysteresis.

2.4. Speed of sound measurement

Longitudinal and shear components of sound speed were measured through the Pulse-Echo method. A Pulser–Receiver (Rigol DG2102) and oscilloscope (Rigol DS1202) were used at room temperature to determine the time difference (Δt) for signal to travel through the sample thickness, which was then translated into velocity. V113-RM (longitudinal) and V205-RM (delay line) transducers were used to transmit and receive signals to measure the longitudinal velocity of sound, and a pair of shear transducers (V156-RM) was used for shear velocity measurement. There were around 2% of uncertainties involved in the measurements.

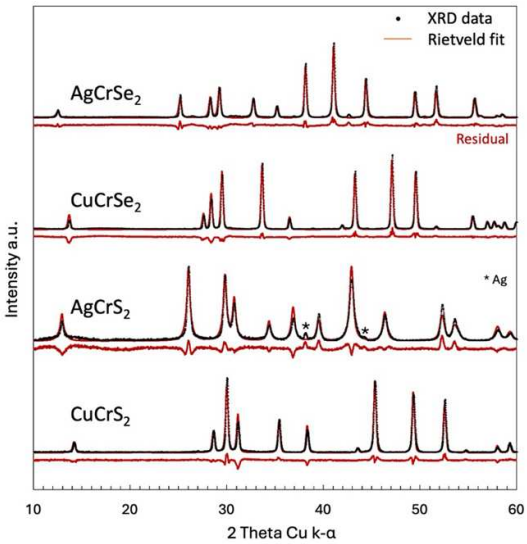

Figure 2. X-ray diffraction patterns at room temperature, superimposed with Rietveld fit (R3m phase) and corresponding residual is shown in red line below each pattern.

3. Results and discussion

3.1. Phase purity and microstructure

Figure 2 shows the x-ray diffraction patterns of $ACrX_2$ samples after SPS, and the corresponding Rietveld fits using the reported structures [33, 37–39]. At room temperature, all four samples are in the ordered $R3m$ structure. The lattice parameters obtained from the Rietveld refinements are shown in table S1 and they agree well with prior literature. For $CuCrSe_2$, Yan *et al* [34] reported that $CuCr_2Se_4$ impurities could be prevented by ball milling for 3 h before SPS. We found this to be correct; only samples with extended ball milling times were found to be $CuCr_2Se_4$-free after final reaction and consolidation in the SPS process. A small amount of elemental Ag as a secondary phase was observed in $AgCrS_2$. Furthermore, the peak width in $AgCrS_2$ is higher than that in the other samples, suggesting the presence of micro strain or nano-sized grains. We also refined the preferred orientation along the [001] direction and found that the March coefficients vary between 0.61 (in $AgCrSe_2$) and 0.88 (in $CuCrSe_2$).

After SPS, the relative densities (ρ_R) of the samples were high (96%–98%), with the exception of the $AgCrS_2$ sample, which had $\rho_R = 93.5\%$. SEM images, shown in figure 3, were collected on fractured surfaces (along the applied pressure direction) of the samples to observe the difference in grain morphology and porosity. Both of the selenide samples appear fully dense with well-formed crystallites. Visual inspection shows that the grain sizes (≈50–100 μms) in the $AgCrSe_2$ sample are significantly larger than that in the $CuCrSe_2$ sample (≈1–10 μms). In both samples, the grain size before and after SPS remains in a similar range (see figure S1), which indicates not much grain growth during consolidation. In the case of $AgCrSe_2$, the grains after SPS show clear signs of plastic deformation, which can be attributed to the formation of shear layers by dislocation slip in the (001) planes [40]. This suggests that in the $AgCrSe_2$ sample, densification occurred mainly by plastic deformation, rather than by diffusion and grain growth, resulting in a sample with significant texturing. This is consistent with the evidence of texturing in XRD refinements. In contrast, evidence of plastic deformation is not visible in the spark plasma sintered $CuCrSe_2$ sample. Both sulfide samples have smaller average grain size than the selenides, and the grains are more difficult to distinguish at the magnification shown in figure 3. The porosity seen in $AgCrS_2$ (dark spots) is consistent with the relatively low geometric density of that sample.

3.2. Thermal diffusivity and latent heat

When converting from thermal diffusivity, D, to thermal conductivity, κ_{total}, using $D = \kappa_{total}/(\rho \times C_p)$, it is common practice to employ the temperature-independent DP approximation for the heat capacity, C_p. While it is well known that DP underestimates C_p at high temperature, the use of this approximation removes the experimental uncertainty associated with the C_p measurement, and thus has the advantage of allowing straightforward comparison of κ_{total} measured by different groups. Indeed, uncertainty in high-temperature C_p measurements has previously been shown to be the largest source of uncertainty in the experimentally reported κ_{total} [41]. Take $AgCrSe_2$, for example, which has been studied by several different research groups.

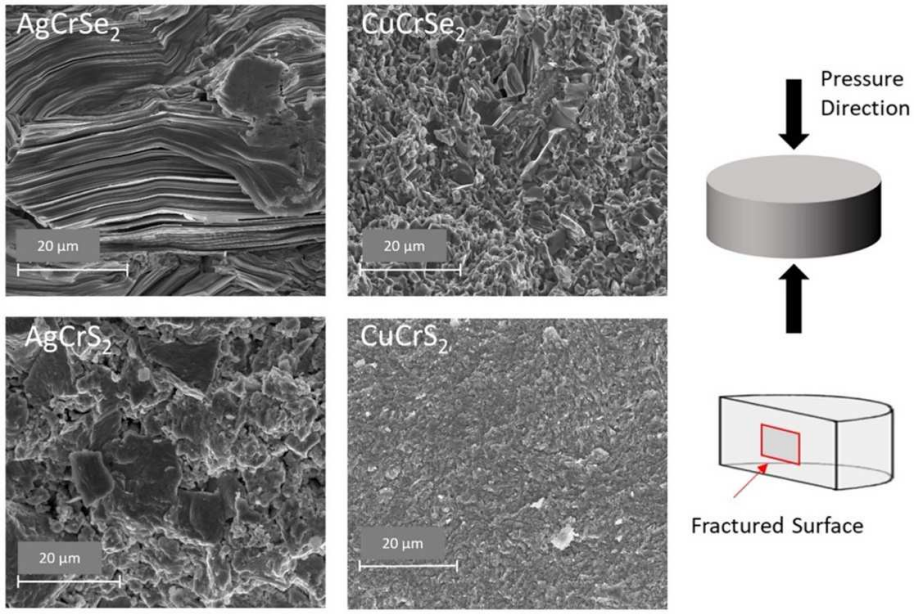

Figure 3. SEM images of the fracture surface of consolidated samples show differences in texturing and grain size ranging from <1 μm in $CuCrS_2$ to >50 μm in $AgCrSe_2$. The applied pressure during spark plasma sintering (SPS) is oriented along the vertical axis in all images, as shown in the schematic on the right.

Figure 4(a) shows the thermal diffusivity of $AgCrSe_2$ from our sample, alongside reports from Gascoin *et al* [8] and Bhattacharya *et al* [11]. The samples were reported to be synthesized with similar procedures and the grain size was reported to be in the range of 10 μm—30 μm by Bhattacharya *et al.* As expected, the diffusivity of the three samples is similar in magnitude across most of the measured temperature range. In contrast, figure 4(b) compares the experimental heat capacity from three prior reports (note, we did not measure the heat capacity in this study), which vary by more than a factor of three. Since the samples nominally have the same compositions, and C_p is not a function of microstructure or other processing-related factors, this large disparity in C_p can only arise from measurement uncertainty. In figure 4(d), we can see the large difference in the magnitude of κ_{total} of $AgCrSe_2$ (0.2 W mK^{-1} vs 0.41 W mK^{-1}) from Gascoin [8] and Bhattacharya [11], respectively, arising primarily from the disparity in C_p. Similar variation in results obtained from different sources (figure S2) is also observed for $CuCrSe_2$ [11, 34].

Unfortunately, directly employing the DP approximation is also not a reasonable approach for $ACrX_2$ compounds, due to the very large latent heat of the SIT, which is seen as a peak in the experimental heat capacity. The inverted peak seen in the thermal diffusivity, caused by the sample absorbing heat during the phase transition, is the mirror image of the C_p peak. Taking the product of D and C_p (along with the density, which does not have any discontinuity at the phase transition), yields thermal conductivity *with no discontinuity* at the phase transition temperature. For this reason, accounting for the experimental latent heat is necessary to obtain an accurate κ_{total}, and thus an accurate zT.

In the current study, we have decided to use a hybrid approach. For $AgCrSe_2$, we employed an 'adjusted C_p' as shown in figure 4(c), obtained by summing the DP C_p and the latent heat of the superionic transition. The latter was estimated based on the peak in the experimental heat capacity reported by Li.B. *et al* [13]. The resulting total thermal conductivity (κ_{total}) using the adjusted C_p is shown in figure 4(d), along with the calculated data from [8] and [11]. In this study, we used a similar approach for the other three compositions, as discussed below. We note that the Debye temperature, θ_D, for $AgCrSe_2$, $CuCrSe_2$, $AgCrS_2$ and $CuCrS_2$ were calculated to be 172 K, 198 K, 157 K and 261 K respectively, using the cubic root average speed of sound [42, 43]. As θ_D for all the compounds is below room temperature, DP approximation is reasonable to apply.

3.3. Transport properties in $ACrX_2$

Figures 5(a)–(d) show the thermal and electronic transport properties for the $CuCrSe_2$ and $AgCrSe_2$ samples from 300 K to 673 K and for $CuCrS_2$ and $AgCrS_2$ samples from 300 K to 773 K. Figure 5(a) shows the total thermal conductivity (κ_{total}) of the all the samples during the cooling cycle. The symbols show κ_{total} calculated using the adjusted C_p described above, which includes an estimated latent heat peak. These κ_{total} values were used when calculating zT. The dashed curves show the 'raw' κ_{total} obtained using a simple DP approximation, which are shown for reference, and also to highlight the phase transition temperatures of

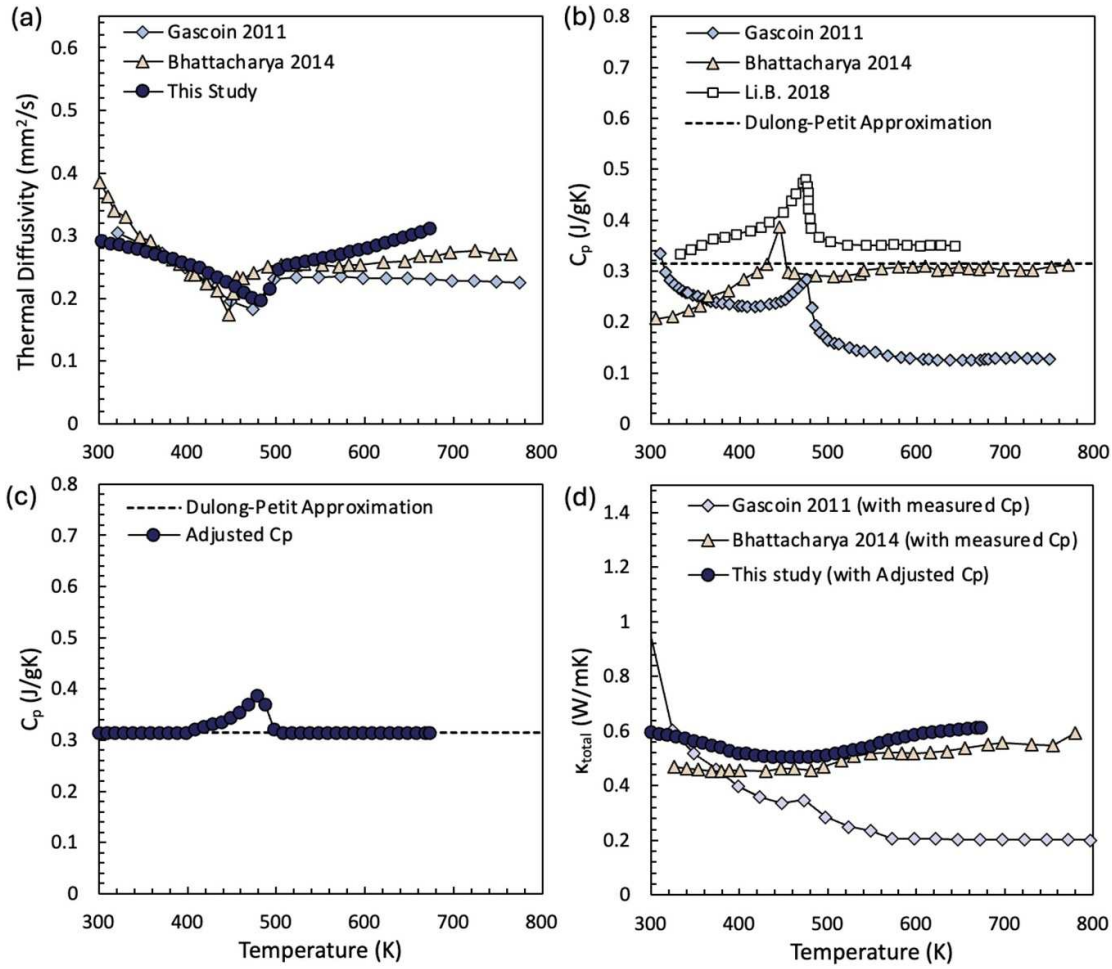

Figure 4. Comparison among literature reports for (a) thermal diffusivity, (b) specific heat C_p, and (d) total thermal conductivity (κ_{total}) for $AgCrSe_2$. κ_{total} in this study was calculated using the adjusted C_p shown in panel (c), which is the sum of the Dulong Petit value and the estimated latent heat.

365 K, 475 K, 683 K and 713 K for $CuCrSe_2$, $AgCrSe_2$, $CuCrS_2$ and $AgCrS_2$, respectively. This is in reasonable agreement with our previous work using differential scanning calorimetry from [17], which is shown in figure S4. We took multiple thermal diffusivity measurements of the LFA, with one heating and one cooling cycle each, shown in figures S11 and S12.

The electrical resistivity (ρ) and Seebeck coefficients (S) of $ACrX_2$ compounds as a function of temperature are shown in figures 5(b) and (c), which agrees well with previous reports [8, 11, 34, 47] (both heating and cooling cycle data is shown in figure S11). The phase transition does not cause any visible discontinuity in the electronic properties of any of the samples. The positive Seebeck coefficients suggest hole-dominated transport, consistent with prior reports [8, 26, 37, 48]. The decrease in Seebeck coefficient up to T_c for $AgCrSe_2$ can be attributed to more charge carriers being excited with increase in temperature, leading to a smaller overall voltage difference generation. For $CuCrSe_2$, ρ and S increase as a function of temperature, which is behavior typical for a degenerate semiconductor. Here, the thermoelectric figure of merit, $zT = S^2T/\rho\kappa$ [49, 50], reaches 0.8 at 673 K, which was experimentally the highest figure of merit reached for this study, and agrees well with previous reports on zT [11, 34, 47]. We note that the mild texturing along the [001] direction in the samples (due to SPS processing) likely leads to slightly anisotropic properties, which were not characterized in the present study, nor in other studies, to our knowledge. We would expect texturing to lead to a slightly inflated zT value in this study and in others.

The electrical resistivity of $AgCrSe_2$, which is more than an order of magnitude higher than $CuCrSe_2$, has an unusual temperature dependence that suggests a transition from non-degenerate to degenerate semiconducting behavior at approximately 475 K. Figure 5(d) shows that $AgCrSe_2$ reached a zT value of 0.23 at 673 K, which is comparable to zT value of 0.29 obtained by Gascoin *et al* using Dulong–Petit approximation. This is much lower than $zT = 0.79$ obtained by Gascoin *et al* [8] using experimental C_p. The lower zT of the Ag-analogue stems from its relatively low mobility compared with the $CuCrSe_2$. On the other hand, both $AgCrS_2$ and $CuCrS_2$ compounds exhibit non-degenerative semiconducting behavior and are

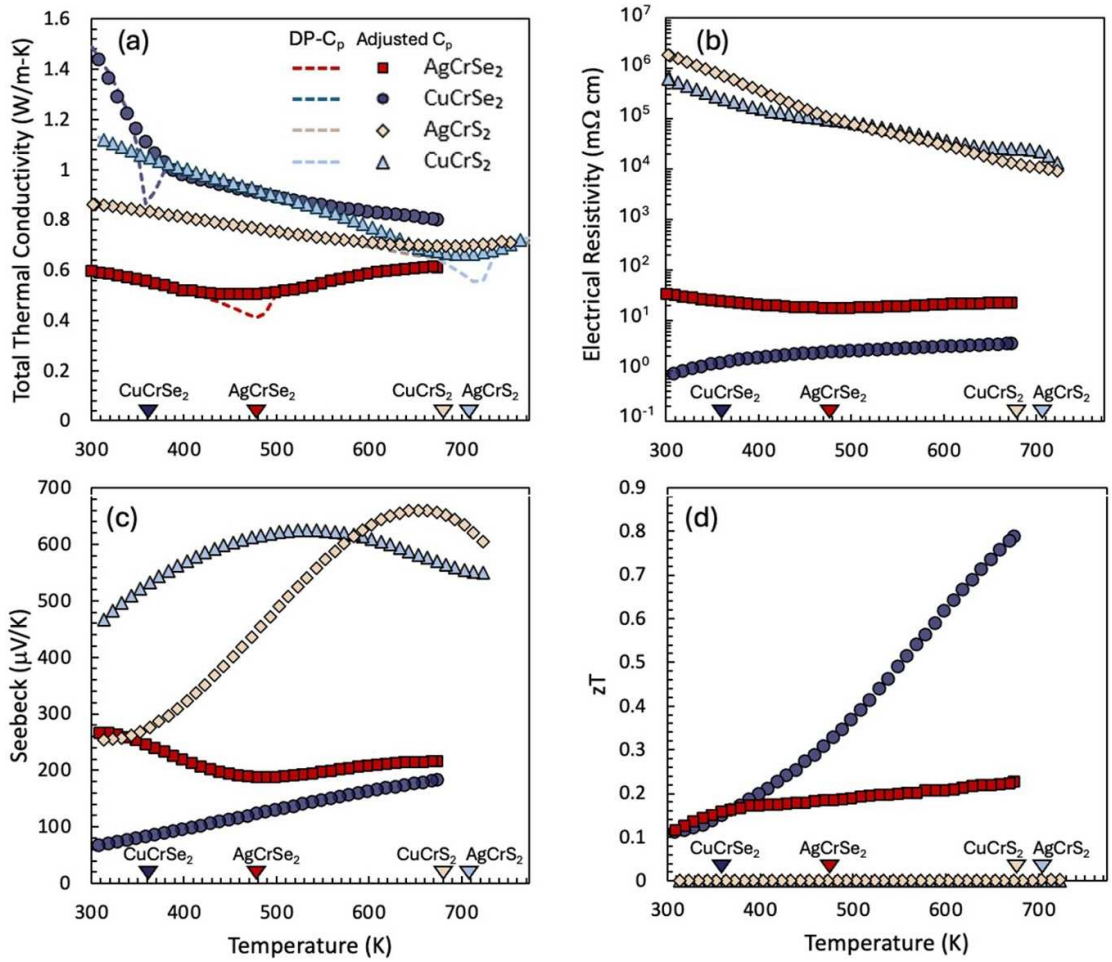

Figure 5. (a) Total thermal conductivity of $ACrX_2$ samples (on the basis of work by [44, 45], we estimate a ±10% uncertainty should be considered) during cooling cycle. The superionic transition temperatures for the compounds are shown with the color-coded arrows. (b) Resistivity (±8% uncertainty), (c) seebeck coefficient (±6% uncertainty) and (d) thermoelectric figure of merit (zT) for $CuCrSe_2$, $AgCrSe_2$, $AgCrS_2$ and $CuCrS_2$ samples are shown here as a function of temperature (±15–19% uncertainty should be considered according [44, 46]). Data was collected on heating and cooling cycle, and the latter one is presented here.

highly resistive at room temperature (several orders of magnitude higher than that of the selenide samples). This leads to a near-zero figure of merit but makes them more interesting as potential superionic materials for solid state batteries [51–53].

The temperature-dependent Hall carrier concentration, n_H, and Hall mobility, μ_H, are shown in figures S7 and S8. At room temperature, the carrier concentrations of $CuCrSe_2$ ($\approx 2 \times 10^{20}$ cm^{-3}) and $AgCrSe_2$ ($\approx 1 \times 10^{20}$ cm^{-3}) are orders of magnitude higher than $CuCrS_2$ ($\approx 2 \times 10^{14}$ cm^{-3}) and $AgCrS_2$ ($\approx 5 \times 10^{14}$ cm^{-3}), explaining the lower electrical conductivity in the latter compounds. While n_H of $CuCrSe_2$ and $AgCrSe_2$ do not vary much with increasing temperature, in $CuCrS_2$ and $AgCrS_2$, n_H increases with temperature and reaches around 10^{17} cm^{-3} and 10^{16} cm^{-3} at 720 K respectively. There is higher uncertainty and scatter in the n_H data for $AgCrS_2$, which is why it was plotted separately in figure S8(a) for more clarity. Regarding mobility, $AgCrSe_2$ exhibited low values in the range of single digit cm^2 Vs^{-1} throughout the entire temperature range. $CuCrS_2$ (≈ 64 cm^2 Vs^{-1} at 323 K) showed roughly similar behavior of mobility to $CuCrSe_2$ (≈ 26 cm^2 Vs^{-1} at 323 K), as the mobility decreases with temperature for both samples. $CuCrSe_2$ shows a semi-linear decrease in mobility with temperature, which is most likely indicative of electron-phonon scattering, while $AgCrSe_2$ displays more temperature-independent mobility, suggesting a stronger presence of scattering of electrons on charge-neutral point defects. The overall low mobilities are consistent with prior reports [12, 38].

Figures S9(a)–(c) shows the Seebeck coefficient, mobility, and zT as a function of carrier concentration (n_h). A single parabolic band model with the assumption of acoustic phonon scattering [54] was used to calculate the effective mass for $AgCrSe_2$ (3.56 m_0) and $CuCrSe_2$ (1.23 m_0) at 323 K and predict the n_h dependence of the electronic transport properties. Based on our limited data, the intrinsic mobility of

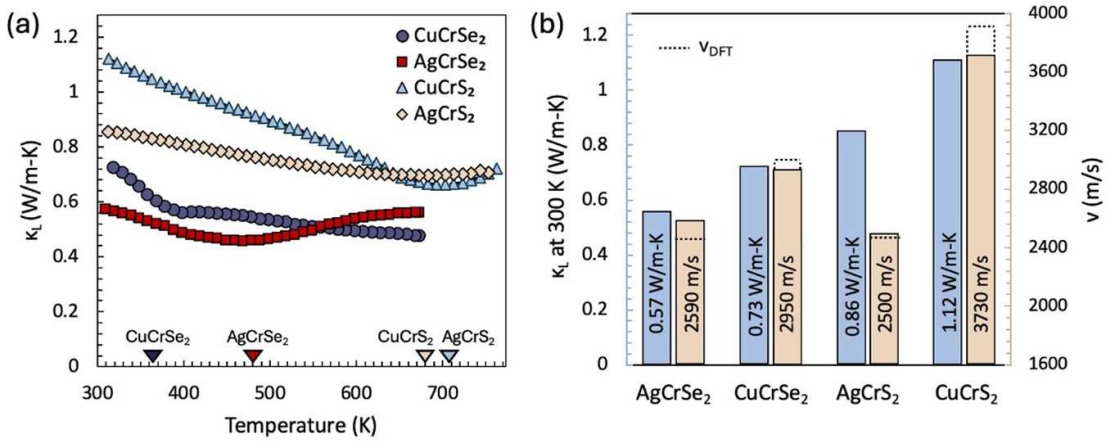

Figure 6. (a) Lattice thermal conductivity (κ_l) of $ACrX_2$ compounds; κ_l was obtained from the difference between experimentally obtained κ_{total} and κ_e (shown in figure S6). Fitted κ_l as a function of temperature, which was obtained by polynomial fitting of experimentally obtained κ_{total}, excluding the value points adjacent to phase transition, is shown as dotted black line. (b) Trend in room temperature κ_l (tan colored columns) and arithmetic average speed of sound (blue columns) for the compounds (uncertainty was less than ±2% considering uncertainty in time and sample thickness measurement). The dashed line represents calculated average speed of sound using DFT [17]. It should be noted that $AgCrS_2$ exhibits surprisingly lower speed of sound, which is consistent with prior DFT calculation.

$AgCrSe_2$ is much lower than that of $CuCrSe_2$, which is the main reason for the smaller predicted peak zT values. Fig S9(c) suggests that the best zT values for $AgCrSe_2$ and $CuCrSe_2$ can be achieved at $n_h = 1.3 \times 10^{20}$ cm^{-3} and $n_h = 2.5 \times 10^{19}$ cm^{-3} respectively. Existing literature data on Seebeck and Hall mobility [34, 38, 47] for $CuCrSe_2$ are presented here for comparison, and the values are found to be in good agreement.

3.4. Trends in lattice thermal conductivity

Figure 6(a) shows the temperature-dependent lattice thermal conductivity, κ_l, of the $ACrX_2$ compounds, obtained from the difference between experimental κ_{total} and κ_e data ($\kappa_l = \kappa_{total} - \kappa_e$). Here, κ_e (shown in figure S6) was calculated from the Wiedemann-Franz law, $\kappa_e = LT/\rho$, where L is the Lorenz number determined from the Seebeck coefficient, L = 1.5 + exp (-|S|/116) [55]. $CuCrSe_2$ is the only sample with significant electronic thermal conductivity ($\kappa_e \approx 0.4$ W mK^{-1} at 300 K), while κ_e is very small for $AgCrSe_2$ ($\kappa_e \approx 0.06$ W mK^{-1}) and for $AgCrS_2$ and $CuCrS_2$, it is almost zero. The relative κ_e and κ_l contributions are shown in figure S5.

At room temperature, all of the samples show relatively low κ_l, ranging from 0.6 W mK^{-1} in $AgCrSe_2$ to 1.1 W mK^{-1} in $CuCrS_2$. Ding *et al* have previously shown that the thermal transport in $ACrX_2$ compounds is dominated by low frequency acoustic phonons [10], and these are particularly important at high temperature, as they persist above the order–disorder transition. At room temperature, we find that the κ_l of the $ACrX_2$ samples is correlated with the average speed of sound (increasing speed of sound leads to increasing κ_l). The exception is $AgCrS_2$, which has a lower speed of sound than the other compounds, including the heavier selenides (see figure 6(b)). The lower speed of sound in $AgCrS_2$ stems from its softer elastic moduli, which was also confirmed by theoretical calculations [10] and in general, compounds with Ag–S bonds have been reported to have extremely soft bonding and correspondingly low speed of sound [6, 56].

A comparison of the longitudinal and shear speed of sound from experiments and DFT calculations is shown in figure S10. Note that the experimental speed of sound of the selenides and the DFT results were reported earlier in [17], while the experimental speed of sound of the sulfides is presented here for the first time. Overall, we note that the $ACrX_2$ samples have a significantly higher speed of sound than other Ag and Cu-based SICs [6, 57–63], which can likely be attributed to the octahedral CrX_2 layers. We used the experimental speed of sound values to estimate the Grüneisen parameters for each compound, given in table S2, following the approach in [64]. $AgCrS_2$ has the highest Grüneisen parameter, among the four compounds. The fact that κ_l in $AgCrS_2$ is not lower than the other compounds in the series, despite its lower speed of sound and higher Grüneisen parameter, is unusual. This might point to a difference in the order parameter, stemming from the higher T_c of $AgCrS_2$ (thus less disorder on the Ag site at room temperature), or potentially from microstructural factors.

Consistent with prior reports for $AgCrSe_2$ and $CuCrSe_2$, the phase transition itself does not appear to have a large impact on κ_l. Even though the activation energy decreases and ionic conductivity increases in the disordered phase, we do not see any significant change in lattice thermal conductivity. Indeed, κ_l has only a weak temperature dependence across the entire measured temperature range, more typical of glass-like, diffusion dominated transport. This can be due to a confluence of factors, most importantly (i) strong anharmonicity suppressing all but the longest wavelength phonons, and (ii) disorder on the cation site beginning at temperatures well below the SIT temperature. Niedziela *et al* have previously shown that the flat κ_l in $AgCrSe_2$ can be modeled by a gradual increase in disorder approaching the phase transition temperature [14], which supports this hypothesis.

4. Conclusion

The present work investigated the experimental thermoelectric properties of layered $ACrX_2$ chalcogenides, including $AgCrSe_2$, $CuCrSe_2$, $AgCrS_2$ and $CuCrS_2$. The measured high-temperature electronic and thermal properties of the selenides were consistent with prior investigations, which showed degenerate semiconductor behavior and low lattice thermal conductivity, resulting in zT maxima of 0.2 and 0.8 for the Ag and Cu analogues, respectively. Ultimately, we showed that the greatest source of potential uncertainty in zT is the heat capacity. In the present study, we therefore decided to use a modified Dulong–Petit heat capacity, to allow reliable comparison between the four different compounds. The high-temperature transport properties of the sulfides were reported here for the first time. We showed them to be electrically insulated due to very low carrier concentrations, and we found that they exhibit slightly higher lattice thermal conductivity than the selenides. Overall, the lattice thermal conductivity of the four $ACrX_2$ compounds could be correlated with the sound velocities of the samples. However, $AgCrS_2$ is an exception; it exhibits sound velocity lower than any other $ACrX_2$ compound, while still maintaining higher lattice thermal conductivity than the selenide compounds. Furthermore, although the samples vary quite drastically in microstructure and grain size, this does not apparently play a strong role in determining the lattice thermal conductivity. Lastly, as reported by other authors, we do not see a decrease in lattice thermal conductivity at the order–disorder phase transition, suggesting that a high degree of disorder and anharmonicity in the low temperature phase already fully suppresses the phonon contributions to thermal transport. There is potential to extend this work by studying the influence of variation in microstructure on lattice thermal conductivity and corresponding effects through the phase transitions. Furthermore, the relatively low sound velocity in $AgCrS_2$, compared with isostructural compounds, would be an interesting focus of additional research, to give a complete understanding of the thermal transport behavior in this layered material group.

Data availability statement

All data that support the findings of this study are included within the article (and any supplementary files).

Acknowledgment

The authors would like to thank the DMREF collaborators from Harvard University, Duke University and North Carolina State University for fruitful discussions regarding microstructure and surface morphology, and meaningful suggestions throughout this study.

Funding

A Z and M T R acknowledge funding from NSF (DMREF Award No. 2118463). A A S acknowledges funding from NSF (DMR SSMC Award No. 2045122). E S T and K C acknowledge NSF (HDR Award No. 2118201).

ORCID iDs

Md Towhidur Rahman https://orcid.org/0009-0000-7340-440X
Kamil Ciesielski https://orcid.org/0000-0002-9787-5967

References

[1] Mahan G D and Roth W L 1976 *Superionic Conductors* (Plenum Press)
[2] Salamon M B 1979 *Physics of Superionic Conductors* (Springer-Verlag)
[3] Boyce J B and Huberman B A 1979 Superionic conductors: transitions, structures, dynamics *Phys. Rep.* **51** 189–265
[4] Zhou Y, Xiong S, Zhang X, Volz S and Hu M 2018 Thermal transport crossover from crystalline to partial-crystalline partial-liquid state *Nat. Commun.* **9** 4712

[5] Yu J, Hu H, Zhuang H-L, Li H and Li J-F 2024 Stabilization of Superionic Copper Selenide Based Thermoelectric Materials *Acc. Mater. Res.* **5** 1428–39
[6] Bernges T *et al* 2022 Considering the role of ion transport in diffuson-dominated thermal conductivity *Adv. Energy Mater.* **12** 2200717
[7] Cheng Z, Zahiri B, Ji X, Chen C, Chalise D, Braun P V and Cahill D G 2021 Good solid-state electrolytes have low, glass-like thermal conductivity *Small* **17** 2101693
[8] Gascoin F and Maignan A 2011 Order-disorder transition in $AgCrSe_2$: a new route to efficient thermoelectrics *Chem. Mater.* **23** 2510–3
[9] Castañeda M, Gutiérrez-Velásquez E I, Aguilar C E, Neves Monteiro S, Amell A A and Colorado H A 2022 Sustainability and circular economy perspectives of materials for thermoelectric modules *Sustainability* **14** 5987
[10] Ding J *et al* 2020 Anharmonic lattice dynamics and superionic transition in $AgCrSe_2$ *Proc. Natl Acad. Sci.* **117** 3930–7
[11] Bhattacharya S *et al* 2014 High thermoelectric performance of $(AgCrSe_2)_{0.5}(CuCrSe_2)_{0.5}$ nano-composites having all-scale natural hierarchical architectures *J. Mater. Chem. A* **2** 17122–9
[12] Romanenko A I, Chebanova G E, Katamanin I N, Drozhzhin M V, Artemkina S B, Han M-K, Kim S-J and Wang H 2022 Enhanced thermoelectric properties of polycrystalline $CuCrS_{2-x}Se_x$($x = 0, 0.5, 1.0, 1.5, 2$) samples by replacing chalcogens and sintering *J. Appl. Phys.* **55** 135302
[13] Li B *et al* 2018 Liquid-like thermal conduction in intercalated layered crystalline solids *Nat. Mater.* **17** 226–30
[14] Niedziela J L, Bansal D, May A F, Ding J, Lanigan-Atkins T, Ehlers G, Abernathy D L, Said A and Delaire O 2019 Selective breakdown of phonon quasiparticles across superionic transition in $CuCrSe_2$ *Nat. Phys.* **15** 73–78
[15] Gautam U K, Seshadri R, Vasudevan S and Maignan A 2002 Magnetic and transport properties, and electronic structure of the layered chalcogenide $AgCrSe_2$ *Solid State Commun.* **122** 607–12
[16] Peng J, Liu Y, Pan Y, Wu J, Su Y, Guo Y, Wu X, Wu C and Xie Y 2020 Fast lithium ion conductivity in layered (Li-Ag)CrS_2 *J. Am. Chem. Soc.* **142** 18645–51
[17] Ding J, Rahman M T, Mao C, Niedziela J L, Bansal D, May A F, Abernathy D L, Ren Y, Zevalkink A and Delaire O 2025 Atomic dynamics in $MCrX_2$ (M = Ag,Cu;X = S,Se) across magnetic and superionic transitions *Phys. Rev. Mater.* **9** 35402
[18] Wood B C *et al* 2021 Paradigms of frustration in superionic solid electrolytes *Phil. Trans. R. Soc. A* **379** 20190467
[19] Li L, Peng C, Chen J, Ma Z, Chen Y, Li S, Wang J and Wang C 2021 Study the effect of alloying on the phase transition behavior and thermoelectric properties of Ag_2S *J. Alloys Compd.* **886** 161241
[20] Rettie A J E, Malliakas C D, Botana A S, Hodges J M, Han F, Huang R, Chung D Y and Kanatzidis M G 2018 Ag_2Se to KAg_3Se_2: suppressing order–disorder transitions via reduced dimensionality *J. Am. Chem. Soc.* **140** 9193–202
[21] Murphy D W, Chen H S and Tell B 1977 Superionic conduction in $AgCrS_2$ and $AgCrSe_2$ *J. Electrochem. Soc.* **124** 1268
[22] Bailey T P and Uher C 2017 Potential for superionic conductors in thermoelectric applications *Curr. Opin. Green Sustain. Chem.* **4** 58–63
[23] Shen X *et al* 2024 Amorphous-like ultralow thermal transport in crystalline argyrodite Cu_7PS_6 *Adv. Sci.* **11** 2400258
[24] Wang C, Cheng R and Chen Y 2023 Theoretical evaluation of the persistence of transverse phonons across a liquid-like transition in superionic conductor KAg_3Se_2 *Chem. Mater.* **35** 1780–7
[25] Wang C and Chen Y 2023 Anisotropic phonon scattering and thermal transport property induced by the liquid-like behavior of $AgCrSe_2$ *Nano Lett.* **23** 3524–31
[26] Brüesch P, Hibma T and Bührer W 1983 Dynamics of ions of the two-dimensional superionic conductor $AgCrS_2$ *Phys. Rev. B* **27** 5052–61
[27] Korotaev E V, Syrokvashin M M, Filatova I Y and Sotnikov A V 2021 Effect of the order-disorder transition on the electronic structure and physical properties of layered $CuCrS_2$ *Materials* **14** 2729
[28] Rana K S, Singh A, Bhui A, Biswas K and Soni A 2024 Anharmonic phonon vibrations of Ag and Cu for poor lattice thermal conductivity in superionic $AgCrSe_2$ and $CuCrSe_2$ *ACS Appl. Energy Mater.* **7** 5621–8
[29] Wang C and Chen Y 2020 Highly selective phonon diffusive scattering in superionic layered $AgCrSe_2$ *npj Comput. Mater.* **6** 26
[30] Xie L, Feng J H, Li R and He J Q 2020 First-principles study of anharmonic lattice dynamics in low thermal conductivity $AgCrSe_2$: evidence for a large resonant four-phonon scattering *Phys. Rev. Lett.* **125** 245901
[31] Yano R and Sasagawa T 2016 Crystal growth and intrinsic properties of $ACrX_2$ (A = Cu, Ag; X = S, Se) without a secondary phase *Cryst. Growth Des.* **16** 5618–23
[32] Hibma T 1980 *The Mixed Conductor Properties of $AgCrS_2$* Vol. 33 (Pergamon Press Ltd)
[33] Tewari G C, Tripathi T S and Rastogi A K 2010 Effect of chromium disorder on the thermoelectric properties of layered-antiferromagnet $CuCrS_2$ *Z. Kristallogr.* **225** 471–4
[34] Yan Y, Guo L, Zhang Z, Lu X, Peng K, Yao W, Dai J, Wang G and Zhou X 2017 Sintering temperature dependence of thermoelectric performance in $CuCrSe_2$ prepared via mechanical alloying *Scr. Mater.* **127** 127–31
[35] Borup K A, Toberer E S, Zoltan L D, Nakatsukasa G, Errico M, Fleurial J-P, Iversen B B and Snyder G J 2012 Measurement of the electrical resistivity and Hall coefficient at high temperatures *Rev. Sci. Instrum.* **83** 123902
[36] Iwanaga S, Toberer E S, LaLonde A and Snyder G J 2011 A high temperature apparatus for measurement of the Seebeck coefficient *Rev. Sci. Instrum.* **82** 063905
[37] Engelsman F M R, Wiegers G A, Jellinek F and Van Laar B 1973 Crystal structures and magnetic structures of some metal(I) chromium(III) sulfides and selenides *J. Solid State Chem.* **6** 574–82
[38] Tewari G C, Karppinen M and Rastogi A K 2013 Effects of competing magnetic interactions on the electronic transport properties of $CuCrSe_2$ *J. Solid State Chem.* **198** 108–13
[39] Bongers P F, Van Bruggen C F, Koopstra J, Omloo W P F A M, Wiegers G A and Jellinek F 1968 Structures and magnetic properties of some metal (I) chromium (III) sulfides and selenides *J. Phys. Chem. Solids* **29** 977–84
[40] Ge B, Li R, Zhu M, Yu Y and Zhou C 2024 Deformation mechanisms of inorganic thermoelectric materials with plasticity *Adv. Energy Sustain. Res.* **5** 2300197
[41] Wang H *et al* 2015 International round-robin study of the thermoelectric transport properties of an n-type half-heusler compound from 300 K to 773 K *J. Electron. Mater.* **44** 4482–91
[42] Toberer E S, Zevalkink A and Snyder G J 2011 Phonon engineering through crystal chemistry *J. Mater. Chem.* **21** 15843–52
[43] Isotta E *et al* 2023 Elastic moduli: a tool for understanding chemical bonding and thermal transport in thermoelectric materials *Angew. Chem. Int. Ed.* **62** e202213649
[44] Heremans J P and Martin J 2024 Thermoelectric measurements *Nat. Mater.* **23** 18–19

[45] Alleno E et al 2015 Invited Article: a round robin test of the uncertainty on the measurement of the thermoelectric dimensionless figure of merit of $Co_{0.97}Ni_{0.03}Sb_3$ *Rev. Sci. Instrum.* **86** 011301
[46] Wang H et al 2013 Transport properties of bulk thermoelectrics: an international round-robin study, part II: thermal diffusivity, specific heat, and thermal conductivity *J. Electron. Mater.* **42** 1073–84
[47] Cheng Y, Yang J, Jiang Q, Fu L, Xiao Y, Luo Y, Zhang D and Zhang M 2015 $CuCrSe_2$ ternary chromium chalcogenide: facile fabrication, doping and thermoelectric properties *J. Am. Ceram. Soc.* **98** 3975–80
[48] Bhattacharya S, Basu R, Bhatt R, Pitale S, Singh A, Aswal D K, Gupta S K, Navaneethan M and Hayakawa Y 2013 $CuCrSe_2$: a high performance phonon glass and electron crystal thermoelectric material *J. Mater. Chem. A* **1** 11289–94
[49] Zevalkink A et al 2018 A practical field guide to thermoelectrics: fundamentals, synthesis, and characterization *Appl. Phys. Rev.* **5** 021303
[50] Shawon A K M A, Guetari W, Ciesielski K, Orenstein R, Qu J, Chanakian S, Rahman M T, Ertekin E, Toberer E and Zevalkink A 2024 Alloying-induced structural transition in the promising thermoelectric compound CaAgSb *Chem. Mater.* **36** 1908–18
[51] Yakshibaev R A, Akmanova G R, Almukhametov R F and Konev V N 1991 Ionic conductivity and diffusion in $CuCrS_2$-$AgCrS_2$ mixed conductors and their alloys *Phys. Stat. Sol. (a)* **124** 417–26
[52] Peng J et al 2021 Stoichiometric two-dimensional non-van der Waals $AgCrS_2$ with superionic behaviour at room temperature *Nat. Chem.* **13** 1235–40
[53] Tewari G C, Tripathi T S and Rastogi A K 2010 Thermoelectric properties of layer-antiferromagnet $CuCrS_2$ *J. Electron. Mater.* **39** 1133–9
[54] Bux S K, Yeung M T, Toberer E S, Snyder G J, Kaner R B and Fleurial J-P 2011 Mechanochemical synthesis and thermoelectric properties of high quality magnesium silicide *J. Mater. Chem.* **21** 12259–66
[55] Kim H-S, Gibbs Z M, Tang Y, Wang H and Snyder G J 2015 Characterization of lorenz number with seebeck coefficient measurement *APL Mater.* **3** 041506
[56] Rathore E, Juneja R, Culver S P, Minafra N, Singh A K, Zeier W G and Biswas K 2019 Origin of ultralow thermal conductivity in n-type cubic bulk $AgBiS_2$: soft Ag vibrations and local structural distortion induced by the Bi_6S_2 lone pair *Chem. Mater.* **31** 2106–13
[57] Lin S, Li W and Pei Y 2021 Thermally insulative thermoelectric argyrodites *Mater. Today* **48** 198–213
[58] Li L et al 2016 High thermoelectric performance of superionic argyrodite compound Ag_8SnSe_6 *J. Mater. Chem. C* **4** 5806–13
[59] Chen J, Sun Q, Bao D, Tian B-Z, Wang Z, Tang J, Zhou D, Yang L and Chen Z-G 2021 Simultaneously enhanced strength and plasticity of Ag_2Se-based thermoelectric materials endowed by nano-twinned CuAgSe secondary phase *Acta Mater.* **220** 117335
[60] Zhao K, Blichfeld A B, Eikeland E, Qiu P, Ren D, Iversen B B, Shi X and Chen L 2017 Extremely low thermal conductivity and high thermoelectric performance in liquid-like $Cu_2Se_{1-x}S_x$ polymorphic materials *J. Mater. Chem. A* **5** 18148–56
[61] Li W, Lin S, Weiss M, Chen Z, Li J, Xu Y, Zeier W G and Pei Y 2018 Crystal structure induced ultralow lattice thermal conductivity in thermoelectric Ag_9AlSe_6 *Adv. Energy Mater.* **8** 1800030
[62] Zhao K, Qiu P, Song Q, Blichfeld A B, Eikeland E, Ren D, Ge B, Iversen B B, Shi X and Chen L 2017 Ultrahigh thermoelectric performance in $Cu_{2-y}Se_{0.5}S_{0.5}$ liquid-like materials *Mater. Today Phys.* **1** 14–23
[63] Kanashiro T, Michihiro Y, Ozaki J, Ohno T and Kojima A 1987 Ultrasonic measurements in the ionic conductor β-Ag_3SI *J. Phys. Soc. Japan* **56** 560–4
[64] Xiao Y et al 2016 Origin of low thermal conductivity in SnSe *Phys. Rev. B* **94** 125203